Volume 1 | Number 1 | Jan 2013 | Pages 1–100

Journal of
Materials Chemistry A

Materials for energy and sustainability
www.rsc.org/materialsA

Li+

ROYAL SOCIETY
OF CHEMISTRY

ROYAL SOCIETY
OF CHEMISTRY

www.rsc.org/materialsA

Journal Name

ARTICLE

Hollow nickel-coated silica microspheres containing rhodium nanoparticles for highly selective production of hydrogen from hydrous hydrazine

Jung Bo Yoo, Han Sol Kim, Seung Hee Kang, Byeongno Lee, and Nam Hwi Hur*

The synthesis of hollow nickel-coated silica microspheres containing rhodium nanoparticles (NPs) (Rh/Ni@SiO$_2$) via thermal hydrolysis of urea using core/shell silica microspheres as templates is described. This dissolution-and-deposition method using urea as a precipitating agent provided uniform hollow microspheres composed of amorphous Ni(OH)$_2$ and silica (SiO$_2$) layers along with small amounts of Rh species even without etching; these hollow microspheres transformed to crystalline Rh/Ni@SiO$_2$ microspheres after annealing at 750 ^{o}C under a reducing atmosphere. The formation of a hollow structure depended on the concentration of urea and unique dissolution behavior of the core/shell silica. The bimetallic Rh/Ni@SiO$_2$ microsphere with a low Rh content (6.35 wt %) is a highly active catalyst for complete dissociation of hydrous hydrazine into hydrogen and nitrogen. Complete release of hydrogen from hydrous hydrazine was accomplished at 25 ^{o}C with H$_2$ selectivity of 99.4 % and turnover number of 66. The used Rh/Ni@SiO$_2$ catalyst, which was recovered by a magnet, was reused in subsequent reactions with virtually identical activity.

Introduction

Combustion of fossil fuels produces large amounts of carbon dioxide (CO$_2$), which is a main contributor to climate change. In contrast, hydrogen (H$_2$) is free of carbon and its combustion produces water as the only waste product. Accordingly, hydrogen plays a major role in the generation of clean energy and reduction of CO$_2$ emissions.[1-3] However, a major drawback is that hydrogen is very difficult to store and transport because it exists as a flammable gas at ambient conditions. An alternative approach is to develop hydrogen storage materials that satisfy several technical requirements, including sufficiently high volumetric and gravimetric capacities, facile release of hydrogen at a reasonably low temperature, and efficient regeneration at a practical temperature.[4] Thus far, a wide range of hydrogen storage materials, such as nano materials,[5] metal hydrides,[6] chemical hydrides,[7] and liquid organic compounds,[8] have been explored to facilitate the use of hydrogen as a fuel. In particular, chemical hydrides composed of boron, nitrogen, and hydrogen atoms have drawn significant interest because they are light atoms with high gravimetric hydrogen capacities. In addition, hydridic B-H and protic N-H bonds can thermally or catalytically dissociate to yield hydrogen. Numerous boron-nitrogen compounds have been evaluated as potential hydrogen-storage materials; they are suitable for producing hydrogen at relatively mild conditions but yield undesired products that cannot be regenerated by hydrogenation under practical conditions.[9-15]

On the other hand, liquid organic hydrogen-storage materials possess significant advantages over solid hydrides,[8] particularly in on-board applications, because they can be handled like fuel in a vehicle. After releasing hydrogen, the dehydrogenated materials can be regenerated by hydrogenation or stored in another tank. However, most of these reversible organic compounds have low gravimetric capacities and require significant energy to dissociate the C-H and N-H bonds. Anhydrous hydrazine (H$_2$NNH$_2$) is a promising hydrogen storage material because it has a high H$_2$ content (12.5 wt %) and is liquid at room temperature. Moreover, it can ideally be dissociated into hydrogen and nitrogen.[16] However, direct use of anhydrous hydrazine is restricted because it is extremely toxic, highly reactive, and even explosive. Hydrous hydrazine, which is prepared by diluting hydrazine with water, is thus used as an alternative to mitigate the toxicity and reactivity of anhydrous hydrazine.[17-20] Complete decomposition of hydrazine yields only hydrogen and nitrogen according to the

following equation: $H_2NNH_2 \rightarrow N_2$ (g) + 2 H_2 (g). Hydrazine can also incompletely decompose into ammonia and nitrogen, as follows: 3 $H_2NNH_2 \rightarrow 4$ NH_3 (g) + N_2 (g). The dissociation pathways depend significantly on the catalyst and reaction conditions. A wide range of catalysts based mostly on metal nanoparticles (NPs) have been developed for complete decomposition of hydrous hydrazine.[21-28] Rh NPs have proven to be very active for the production of H_2 from hydrous hydrazine: Their H_2 selectivity is close to 43 %.[29] Monometallic catalysts containing Co, Ru, or Ir NPs are also active for the decomposition reaction but their selectivity is very low (<7 %). Most Ni-based bimetallic catalysts with precious metals show enhanced selectivity towards H_2 production;[30-35] their activities not only depend on the metal composition but also on the compositional ratio. Thus far, Rh-rich alloy (i.e., Rh_4Ni) shows the highest selectivity (~100%) for the production of H_2 from hydrous hydrazine at room-temperature.[35] However, complete replacement of Rh by abundant metals or reduction of the Rh content by alloying with inexpensive metals is necessary for this technology for producing H_2 from hydrazine to be industrially viable.[36-38]

Thus far, most of the catalysts developed for complete decomposition of hydrous hydrazine are NPs that are typically composed of noble metals and transition metals. Bimetallic NPs have a high surface area, which is very advantageous, particularly for catalytic activity. The synthesis of bimetallic NPs typically requires high temperatures, which lead to agglomeration of the NPs. To prevent aggregation, NPs can be covered with capping agents; however, these often hamper the catalytic reaction. Another drawback is that bimetallic NPs are difficult to separate and reuse in a subsequent reaction mainly because of their extremely small sizes. From this perspective, hollow microspheres containing active-metal NPs on their outer surfaces are a significant challenge both synthetically and catalytically. An important benefit of hollow microspheres is that they can be used as recyclable supports with high surface areas.

Hollow materials containing metal NPs are typically prepared using sacrificial templates.[39-41] This process involves coating the desired materials onto the templates and then etching the templates away to form the hollow structure. In earlier work, we prepared hollow materials through selective etching of the templates using a concentrated alkaline solution.[42] This methodology is simple but partially degrades the active shell components. Reports on the syntheses of hollow materials without etching have thus far been limited. In the present work, we use core/shell silica (SiO_2) microspheres as templates and employ urea as an alkaline medium, thereby forming hollow microspheres that contain metal species without etching. This dissolution-and-deposition method proceeds through thermal hydrolysis of urea. Urea is a simple organic compound that has two NH_2 groups connected by a carbonyl (CO) group; it is neither acidic nor alkaline in water at ambient conditions. Upon heating, however, it produces ammonia in water, which causes the solution to become alkaline. A urea solution at high temperature can dissolve the

silica in a controlled manner even though it is only slightly soluble.[43-52] The weak alkalinity of the urea solution leads to the uniform deposition of metal precursors and gradual dissolution of the silica core.

Herein, we report hollow nickel-coated microspheres containing Rh NPs ($Rh/Ni@SiO_2$) that were prepared by thermal hydrolysis of urea using core/shell silica microspheres as templates followed by annealing at 750 °C under flowing 5% H_2 in Ar. The $Rh/Ni@SiO_2$ microspheres maintain a spherical shape, have large cavities in the core, and contain less than 6.35 wt % Rh. At room temperature, the $Rh/Ni@SiO_2$ catalyst generates H_2 with over 99% selectivity within 1.5 h. Moreover, the used $Rh/Ni@SiO_2$ catalyst recovered by a magnet produces H_2 at the same selectivity; these results generate significant promise for hydrous hydrazine as a potential hydrogen-storage material.

Experimental Section

Chemicals. All chemicals were purchased from commercial suppliers and used without further purification unless otherwise stated. Tetraethyl orthosilicate (TEOS), nickel acetylacetonate ($C_{10}H_{14}NiO_4$), and rhodium chloride hydrate ($RhCl_3 \cdot xH_2O$) were purchased from Tokyo Chemical Industry Co. (Tokyo, Japan). Octadecyl trimethoxysilane (C_{18}-TMS), hydrazine hydrate ($H_2NNH_2 \cdot H_2O$, 98%), benzyl aldehyde, phenol, sodium hypochlorite (NaOCl), sodium hydroxide (NaOH), sodium nitroferricyanide dihydrate ($Na_2[Fe(CN)_5NO] \cdot 2H_2O$), and urea were purchased from Sigma-Aldrich (St Louis, USA). Ethanol, deionized water, sulfuric acid, and ammonia solution (25-28%) were obtained from Samchun Chemical Reagent Co. (Seoul, Korea).

Synthesis of core/shell silica microspheres (core/shell SiO_2). The core/shell silica microsphere templates were prepared using a slightly modified Stöber procedure.[53] In brief, 75 mL of ethanol, 10 mL of deionized water, and 3 mL of ammonia solution were added to a round-bottom flask, and the solution was stirred for 10 min. Using a syringe, TEOS (6 mL) was injected into the solution. After vigorous stirring for 2 h, a mixture of TEOS (5 mL) and C_{18}-TMS (2 mL) was added, and the solution was stirred for another 2 h. White precipitate formed and was separated from the solution by centrifugation. To remove all organic residues in the precipitated powders, the powders were sintered in air at 550 °C for 6 h, yielding 2.0 g of silica powders. The silica has a spherical shape and a core/shell structure. The core diameter is approximately 300 nm and the shell thickness ranges from 20 to 30 nm.[42]

Synthesis of hollow nickel-coated silica microspheres ($Ni@SiO_2$). The prepared core/shell SiO_2 microspheres (0.495 g) were dispersed in 250 mL of deionized water in a 500 mL round-bottom flask. Nickel acetylacetonate (0.4 g, 1.6 x 10^{-3} mol) and urea (4.0 g, 6.7 x 10^{-2} mol) were dissolved into the solution, which was then stirred at 80 °C for 2 h. The white microspheres gradually became green colloidal spheres, which were separated from the solution by centrifugation (3000 rpm), and dried in an oven at 100 °C. The dried microspheres

(Ni(OH)$_2$@SiO$_2$) were annealed at 750 ^{o}C for 20 h under a reducing atmosphere (Ar/H$_2$ = 95:5) to yield the desired nickel-coated microspheres.

Synthesis of hollow nickel-coated silica microspheres containing rhodium (Rh/Ni@SiO$_2$). The procedure for the synthesis of Rh/Ni@SiO$_2$ is virtually identical to that for Ni@SiO$_2$ except that rhodium chloride hydrate is added as a source of Rh. The core/shell SiO$_2$ microspheres (0.495 g) were dispersed in 250 mL of deionized water in a 500 mL round-bottom flask. Rhodium chloride hydrate (0.04 g, 1.9 x 10^{-4} mol), nickel acetylacetonate (0.4 g, 1.6 x 10^{-3} mol), and urea (4.0 g, 6.7 x 10^{-2} mol) were dissolved into the solution, which was then stirred at 80 ^{o}C for 2 h. The white microspheres gradually became green colloidal spheres, which were separated from the solution by centrifugation (3000 rpm), and dried in an oven at 100 ^{o}C. The dried microspheres (Rh/Ni(OH)$_2$@SiO$_2$-1T) were annealed at 750 ^{o}C for 20 h under a reducing atmosphere (Ar/H$_2$ = 95:5). The rhodium-deposited nickel-coated silica microspheres are denoted as Rh/Ni@SiO$_2$-1T. Prior to annealing, the dried microspheres were coated once more in a similar manner. The resulting microspheres were annealed at 750 ^{o}C for 20 h under a Ar/H$_2$ (95:5) atmosphere. These annealed microspheres are denoted as Rh/Ni@SiO$_2$-2T. Similarly, a Rh/Ni@SiO$_2$-3T sample was prepared by repeating the procedure three times.

Hydrogen production from hydrous hydrazine. The evolution of hydrogen from hydrazine was examined using a two-necked round-bottom flask at room temperature; one neck was connected to a gas burette and the other neck was used to inject a solution of hydrazine hydrate. The catalyst (Rh/Ni@SiO$_2$, 50 mg) was loaded into the flask and dispersed in 5.0 mL of deionized water containing 1 mL of 0.5 M NaOH under an Ar atmosphere. Hydrazine hydrate (0.1032 g, 2.06 mmol) was then added to the catalyst via a syringe. Gas evolution was observed immediately. The gases released from the solution first passed through a trap containing sulfuric acid (0.1 M); this trap absorbed ammonia gas, which might be generated by the reaction. The amount of passed gases was volumetrically measured using a gas burette. To determine the amount of NH$_3$ and N$_2$H$_4$ left in the flask after the reaction, the indophenol-blue method was employed. Two solutions were prepared to perform this test. One solution comprised 0.5 g of phenol and 2.83 mg of Na$_2$[Fe(CN)$_5$NO]·2H$_2$O in 50 mL of deionized water and the other comprised 0.251 g of NaOH and 0.15 mL of NaOCl in 50 mL of deionized water. The pH of the solution that remained in the round-bottom flask was adjusted to 7.0 using a 0.1 M H$_2$SO$_4$ solution. Then, 1 mL of the pH-adjusted solution and 5 mL of each of the two solutions were mixed, and the resultant solution was stirred thoroughly for 1 h. The absorbance of the solution was measured and the total concentration was determined using a calibration curve obtained from a standard solution.[54,55] In a similar manner, the amounts of NH$_3$ and N$_2$H$_4$ in the H$_2$SO$_4$ trap were also determined.

Methods. Powder X-ray diffraction (XRD) patterns were recorded using a Rigaku DMAX 2500 diffractometer (Cu Kα;

Rigaku, Japan) operating at 40 kV and 150 mA. Transmission electron microscopy (TEM) was performed using a JEOL JEM-2100F microscope (JEOL, Japan). Specimens for TEM examinations were prepared by dispersing finely ground powders of the samples in anhydrous ethanol and then allowing a drop of the suspension to evaporate on a 400 mesh carbon-coated grid. Energy-dispersive X-ray (EDX) spectroscopy was performed using the same microscope as used for TEM. Line-scan analyses were performed in scanning transmission electron microscope-mode using a real-time interactive imaging system with a high-angle annular dark-field detector. Adsorption and desorption measurements were carried out at 77 K using an ASAP 2420 instrument (Micromeritics, Norcross, USA) with nitrogen as the adsorptive gas. The Brunauer-Emmett-Teller (BET) surface areas were calculated using P/P$_0$ = 0.05 - 0.3 from the adsorption curve using the BET equation. The pore-size distributions were obtained from the desorption curve using the density functional theory method. Prior to each sorption measurement, the sample was out-gassed at 300 ^{o}C for 24 h *in vacuo* to completely remove the impurities. To investigate the elemental compositions, X-ray photoelectron spectroscopy (XPS; Theta probe AR-XPS System, Thermo Fisher Scientific, UK) analysis using a mono-chromated Al Kα x-ray source (hv = 1486.6 eV) was performed at the Korea Basic Science Institute (KBSI) in Busan. Field emission scanning electron microscopy (FE-SEM) was performed using a Hitachi S-4700 microscope at KBSI in Jeonju. The contents of Ni and Rh in Rh/Ni@SiO$_2$ were analyzed using inductively coupled plasma atomic emission spectroscopy (ICP-AES, JY Ultima2C) at KBSI in Seoul.

Results and discussion

Our strategy to prepare hollow microspheres containing nickel hydroxide and rhodium species is illustrated in Fig. 1; this figure schematically represents the process for the synthesis of three different materials starting from core/shell SiO$_2$ microspheres: (a) yolk-shell microspheres with large yolks and thin shells, (b) yolk-shell microspheres with small yolks and thick shells, and (c) hollow microspheres with very thick shells. Our method relies on the thermal hydrolysis of urea to produce a hollow structure. The urea solution containing Rh and Ni precursors readily infiltrates into the silica template via mesopores in the shell. At 80 ^{o}C, urea dissociates into ammonium cations (NH$_4^+$) and hydroxide anions (OH$^-$) according to the following equation: NH$_2$CONH$_2$ + 3 H$_2$O → CO$_2$ + 2 NH$_4^+$ + 2 OH$^-$. The hydroxide anions generated from thermal hydrolysis of urea drive the ionization and dissolution processes on the SiO$_2$ surface. Deposition of Ni^{2+} and Rh^{3+} species appears to occur through electrostatic interactions on the ionized surface of SiO$_2$. Metal species are presumably deposited on the silica shell in their hydroxide forms. Simultaneously, the silica cores gradually dissolve and form the inside of the silica shell. Repetition of this dissolution-and-deposition process eventually leads to the formation of hollow
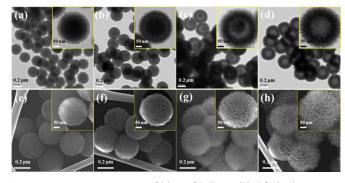
Fig. 1 Schematic representation of the preparation of hollow microspheres via the dissolution-and-deposition pathway using core/shell SiO₂ microspheres as templates: (a) Rh/Ni(OH)₂@SiO₂-1T, (b) Rh/Ni(OH)₂@SiO₂-2T, and (c) Rh/Ni(OH)₂@SiO₂-3T. The cores and shells of the parent SiO₂ template are depicted in dark and light blue, respectively. Rh NPs are represented as red dots. The shells of (a), (b), and (c) are depicted in yellow and blue, which represent Ni(OH)₂ and SiO₂, respectively. The synthesis of Rh/Ni(OH)₂@SiO₂-3T involves three dissolution-and-deposition steps.

Fig. 2 Representative TEM images of (a) core/shell SiO₂, (b) Rh/Ni(OH)₂@SiO₂-1T, (c) Rh/Ni(OH)₂@SiO₂-2T, and (d) Rh/Ni(OH)₂@SiO₂-3T are displayed in the top panels. The bottom panels show SEM images of the corresponding samples, i.e., (e) core/shell SiO₂, (f) Rh/Ni(OH)₂@SiO₂-1T, (g) Rh/Ni(OH)₂@SiO₂-2T, and (h) Rh/Ni(OH)₂@SiO₂-3T. The insets show higher magnifications of the TEM and SEM images.

microspheres, which are composed of Ni(OH)₂, SiO₂, and Rh species. An important benefit of this method is that bimetallic hollow materials can be prepared simply by controlling the dissolution-and-deposition step.

Mavredaki et al. demonstrated that hydroxide ions promote the self-condensation of silicic acid in the pH range of 5-10 to yield dissolved silicate species.[56] Furthermore, this self-condensation process becomes more dominant when metal-hydroxide moieties are present on the SiO₂ surface. Tomiyama et al. also reported that nickel hydroxide particles on silica were prepared through deposition-and-precipitation processes.[57] These reported methods are straightforward; however, it is difficult to use them to achieve the desired shape and functionality. Our approach offers simple and convenient synthesis of hollow structures containing active metal species on the silica surface in a controlled manner. It is worth noting that the Rh/Ni(OH)₂@SiO₂ microspheres cannot be obtained using core SiO₂ microspheres with non-porous shells as templates; these microsphere templates yielded SiO₂ microspheres with irregular deposition of the metal species (Fig. S1). These results clearly suggest that the porous shell also plays a crucial role in the dissolution-and-deposition processes. The cavity size and surface area can be tuned by adjusting the concentration of urea and heating temperature.

Typical TEM and SEM images of core/shell SiO₂, Rh/Ni(OH)₂@SiO₂-1T, Rh/Ni(OH)₂@SiO₂-2T, and Rh/Ni(OH)₂@SiO₂-3T are shown in Fig. 2 and demonstrate the distinctive changes in surface morphology after thermal hydrolysis of urea. The core/shell silica templates (Fig. 2(a)) had average diameters of 300 nm with shell thicknesses ranging from 20 to 30 nm. Fig. 2(b) shows a TEM image of Rh/Ni(OH)₂@SiO₂-1T, which is the first dissolution-and-deposition product; this image clearly illustrates the formation of void space between the shell and core, which suggests that thermal hydrolysis of urea resulted in the slow dissolution of silica. Interestingly, the average diameter of Rh/Ni(OH)₂@SiO₂-1T is slightly larger at ~340 nm. The void space increased in the second dissolution-and-deposition product, Rh/Ni(OH)₂@SiO₂-2T, which had a clear yolk-shell structure. The TEM images shown in Fig. 2(c) reveal that the diameter of the yolk (core) was ~120 nm and the shell thickness drastically increased to about 60-80 nm; this suggests that the core silica gradually dissolved while the shell expanded through

the deposition of dissolved silica as well as the Ni(OH)₂ coating. As illustrated in Fig. 2(d), hollow microspheres with shell thicknesses of ~120 nm formed after three repeated reactions; this clearly demonstrates that the core completely dissolved. The overall diameters of Rh/Ni(OH)₂@SiO₂-3T ranged from 370 to 390 nm and were larger than that of the core/shell silica template. The TEM images suggest that dissolved silica accumulated inside the silica shell while the metal components were coated on the outer shell. This is in good agreement with the increment in diameter of the hollow microspheres.

Representative SEM images of the same samples are shown in the bottom panel of Fig. 2. The overall diameters of the samples were virtually identical to those estimated from the TEM images. The SEM images illustrate that the surface had a unique flower-like morphology. The flower-like surface becomes more distinctive with increasing number of dissolution-and-deposition steps. It has been reported that Ni(OH)₂ grows in flower-like architectures in strongly alkaline solution. It is typically crystalline and shows distinctive XRD patterns corresponding to α- or β-phase Ni(OH)₂. Interestingly, the XRD patterns of the as-prepared samples did not show any distinctive peaks (Fig. S2), which suggests that all the phases in Rh/Ni(OH)₂@SiO₂ were amorphous. Thus far, amorphous Ni(OH)₂ phase with a flower-like morphology has not been reported. This amorphous nature suggests that the dissolved silica might interfere with the formation of a long-range ordered crystalline Ni(OH)₂ phase. Instead, Ni(OH)₂ petals grew along with dissolved silica species on the shell, which resulted in the formation of disordered amorphous Ni(OH)₂. To investigate the elemental distribution and confirm the hollow structure, EDX line scan elemental profiles of the three Rh/Ni(OH)₂@SiO₂ samples were obtained as given in Fig. 3. The results confirm the presence of Ni, Si, and Rh, although the signal intensity of Rh is very low due to the minute amount of Rh in the sample. The EDX scan data clearly show that the intensity of Ni increases with increasing dissolution-and-deposition time while the intensity of Si decreases. In

particular, the intensity of Si in the core is drastically reduced, confirming
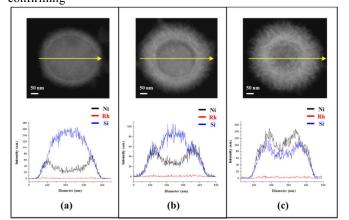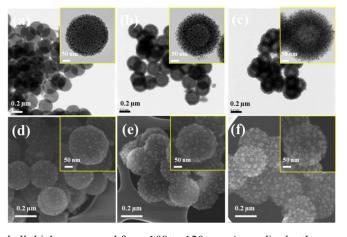

Fig. 3 EDX elemental line scans of (a) Rh/Ni(OH)$_2$@SiO$_2$-1T, (b) Rh/Ni(OH)$_2$@SiO$_2$-2T, and (c) Rh/Ni(OH)$_2$@SiO$_2$-3T. The top panels show the TEM images that include the positions of the line scan (yellow line). The bottom panel shows the EDS signal intensity for Ni, Si, and Rh across the diameter of the corresponding microsphere.

that the sample had a hollow structure. A notable feature in the line-scan curves of Rh/Ni(OH)$_2$@SiO$_2$-3T is that the intensity of Ni is stronger than that of Si, which suggests that Ni(OH)$_2$ was predominantly coated on the outer shell while SiO$_2$ was mostly deposited on the inner shell. The EDX line-scan data are consistent with the TEM and SEM images shown in Fig. 2. The presence of Rh was not clear from the line-scan data but was confirmed by ICP-AES and EDX elemental analyses; this suggests that Rh species were embedded in the shell as tiny NPs. As evident from Table S1, the two techniques yielded slightly different results because of their different measurement methods. We used the ICP-AES analysis data to evaluate the catalytic activity. With increasing dissolution-and-deposition time, the Rh content increased and was roughly proportional to the nominal composition. The maximum amount of Rh in Rh/Ni(OH)$_2$@SiO$_2$-3T was 6.35 wt %. In addition, the presence of Rh and the hollow structure were also evidenced by elemental mapping images shown in Fig. S7.

To obtain crystalline bimetallic Rh/Ni phases, the Rh/Ni(OH)$_2$@SiO$_2$ samples were annealed at 750 °C for 20 h under flowing 5% H$_2$ in Ar, which converted them into hollow Rh/Ni@SiO$_2$ microspheres containing Ni and Rh NPs. As illustrated in the TEM images (Fig. 4), the parent hollow structures were maintained even after heating at high temperatures. Usually, annealing of hollow spheres composed of metal components at high temperatures leads to collapse or shrinkage of the parent hollow structure.[58,59] However, in the case of Rh/Ni(OH)$_2$@SiO$_2$, the hollow shape was retained throughout the heat treatment because of the presence of silica layers in the inner shell, which appear to play a crucial role in maintaining the hollow structure. In addition, the silica layers act as supporting materials for the formation of the Ni layers. During the heating process, small amounts of the Rh species in the shells were deposited onto the abundant Ni surface to form bimetallic NPs. Relative to Rh/Ni(OH)$_2$@SiO$_2$-3T, the diameter

of Rh/Ni@SiO$_2$-3T remained almost constant at 370 nm and the

Fig. 4 The top panel shows TEM images of (a) Rh/Ni@SiO$_2$-1T, (b) Rh/Ni@SiO$_2$-2T, and (c) Rh/Ni@SiO$_2$-3T after heating the as-prepared samples at 750 °C under flowing 5% H$_2$ in Ar. The corresponding SEM images are illustrated in (d) Rh/Ni@SiO$_2$-1T, (e) Rh/Ni@SiO$_2$-2T, and (f) Rh/Ni@SiO$_2$-3T. The insets show higher magnifications.

shell thickness ranged from 100 to 120 nm. Accordingly, the annealed sample retained the hollow structure with a virtually identical shell thickness. However, annealing caused the flower-like surface morphology to disintegrate and large quasi-spherical agglomerates to grow along with the coated Ni layers. Thus, annealing transformed the flower-like Ni(OH)$_2$ phases into large metallic Ni granules and layers. This transformation process is quite similar to the melt-grown agglomeration procedure. The Ni(OH)$_2$ phase deposited on the outer shell melts at ~230 °C and the melted Ni particles initially coat on the surface. Some of the Ni phases agglomerate to form granules on the surface. In contrast, the extent of coarsening of the Rh species was limited, which is mainly because of their high melt temperature. The SEM images show that large Ni granules with spherical shapes protruded from the Ni surface (Fig. 4).

The structures of the bimetallic phases in the shell were characterized by XRD. As illustrated in Fig. 5, XRD patterns of the three Rh/Ni@SiO$_2$ samples show two distinctive peaks at 44.2 and 52.4°, which are typical of the Ni phase (space group: F_{m3m}) with a face-centered cubic structure (JCPDS No. 70-1849).[60-63] The two peaks were assigned to the (111) and (200) reflections. A very broad peak near 20° was assigned to SiO$_2$ (JCPDS No. 29-0085). No diffraction peaks corresponding to Rh appeared even in Rh/Ni@SiO$_2$-3T, which indicates the amount of Rh in the sample was too small to be detected by XRD.[64,65] Another plausible scenario is that Rh alloyed with Ni to yield a Ni-rich bimetallic phase. The XRD data provide indirect evidence of the formation of bimetallic NPs. Namely, a part of the Rh metal was incorporated in the Ni metal to form alloy NPs while the remainder was present in the shell as sub-nanometer Rh NPs. This conjecture is also supported by the XRD patterns of Rh@SiO$_2$, which is shown in Fig. S6.

The oxidation states and chemical environments of Rh, Ni, Si, and O in Rh/Ni@SiO$_2$-1T, Rh/Ni@SiO$_2$-2T, and

Rh/Ni@SiO$_2$-3T were further characterized by XPS. Fig. S3 shows detailed XPS spectra of the important regions (i.e., Rh 3d, Ni 2p, Si 2p, O 1s) for each element. All species of interest
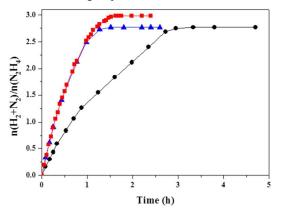

are displayed in

Fig. 5 Powder XRD patterns of (a) Rh/Ni@SiO$_2$-1T, (b) Rh/Ni@SiO$_2$-2T, and (c) Rh/Ni@SiO$_2$-3T. Theoretical XRD patterns of Ni and Rh are also displayed for reference.

the XPS spectra. The Rh 3d signals are observed at 306 and 310 eV, which were assigned to Rh 3$d_{5/2}$ and Rh 3$d_{3/2}$, respectively. The two Rh 3d signals in Rh/Ni@SiO$_2$-3T are substantially more intense than those of Rh/Ni@SiO$_2$-1T, suggesting that the Rh/Ni@SiO$_2$-3T sample contained more Rh. Assignments of the Ni 2p peaks are complicated due to the presence of several Ni species in different chemical environments. Four peaks are displayed at ~857.2, 861.1, 874.8 and 879.7 eV. On the basis of previous reports on Ni metal, the two peaks at 857.2 and 874.8 eV were assigned to Ni 2$p_{3/2}$ and Ni 2$p_{1/2}$, respectively.[66-73] The two broad remaining peaks are presumably associated with NiO or could be ascribed to the satellite peak. The presence of characteristic Ni 2p signals in the Ni 2p XPS spectra indicates that metallic Ni was coated on the outer shell and NiO formed presumably at the boundary between Ni and SiO$_2$. The binding energies of Si 2p and O 1s are very close to the values reported for a range of silicate species.[74-76]

Prior to testing the catalytic activities of Rh/Ni@SiO$_2$-1T, Rh/Ni@SiO$_2$-2T, and Rh/Ni@SiO$_2$-3T, we measured their N$_2$ adsorption and desorption isotherms to estimate their surface areas and pore sizes. Type-IV isotherm curves with distinctive hysteresis loops were observed for all three samples (Fig. S4), which suggests the presence of mesopores in the shells.[77-81] The specific surface areas of the samples were very high and quite similar, ranging from 172.63 to 180.21 m^2/g. However, the pore-size distribution curves show that the pore sizes increased substantially from 4.7 nm in Rh/Ni@SiO$_2$-1T to 5.6 nm in Rh/Ni@SiO$_2$-3T. In addition, Rh/Ni@SiO$_2$-3T had a

considerable number of pores that are 10 nm or larger. This suggests that a greater variety of pores sizes were produced with increasing number of dissolution-and-deposition steps.
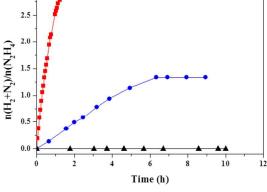
Because of the high specific surface area of the bimetallic

Rh/Ni@SiO$_2$ samples, they were expected to show great

Fig. 6 Production of H$_2$ and N$_2$ from hydrous hydrazine as a function of time in the presence of NaOH (0.5 M) at 25 °C using Rh/Ni@SiO$_2$-1T (black circles), Rh/Ni@SiO$_2$-2T (blue triangles), and Rh/Ni@SiO$_2$-3T (red squares) catalysts.

promise catalytically. Hydrous hydrazine was selected as a substrate to illustrate the selective production of H$_2$ and N$_2$. To determine the efficiency of H$_2$ production using the bimetallic catalyst, we reacted hydrous hydrazine (0.404 M) with the catalyst at 25 °C in a round-bottom flask and measured the production of H$_2$ volumetrically using a gas burette. To ensure that the catalyst surface was basic and prevent the production of unwanted NH$_3$ gas, NaOH (0.5 M) was added to the hydrazine solution. When Rh/Ni@SiO$_2$-1T was used as a catalyst, gases evolved for approximately 3.3 h and the amount of gases released over the course of the reaction was 2.77 equivalents (equiv), as illustrated in Fig. 6. This corresponds to a H$_2$ selectivity of 91.3%. The turnover number (TON) of Rh/Ni@SiO$_2$-1T was about 143, which was calculated on the basis of the Rh content. Under the same reaction conditions, the second catalyst (Rh/Ni@SiO$_2$-2T) yielded 2.78 equiv of gases in 1.6 h and had a 91.4% H$_2$ selectivity (TON = 90). The catalytic activity of Rh/Ni@SiO$_2$-3T towards the same reaction was also tested. Almost complete conversion of hydrazine was achieved in 1.5 h, yielding 2.99 equiv of gases (TON = 66). The selectivity of Rh/Ni@SiO$_2$-3T toward H$_2$ production was remarkably high (99.4%). These results suggest that increasing the Rh content in the Rh/Ni@SiO$_2$ catalyst increases the H$_2$ selectivity as well as the yield. The optimal amount of Rh in the Ni-coated hollow catalyst was ~6.36 wt %, which is remarkably low compared with the values reported previously.[36] In a recent paper by Singh and Xu, it was demonstrated that the H$_2$ selectivity strongly depends on the Rh/Ni ratio in Rh$_x$Ni$_y$ alloys, and the Rh$_4$Ni catalyst with 87.5 wt % Rh reaches a maximum H$_2$ selectivity close to 100%. Thus, Rh/Ni@SiO$_2$-3T could be the catalyst with the lowest Rh content for the selective decomposition of hydrous hydrazine. Its high selectivity at low Rh loadings is unprecedented in RhNi alloys.

For comparison, monometallic catalysts that contain only Ni or Rh, such as $Ni@SiO_2$ and $Rh@SiO_2$, were used as catalysts under the same conditions. As illustrated in Fig. 7, no gas products were obtained when $Ni@SiO_2$ was used as a catalyst.

Even over $Rh@SiO_2$ catalysts, a low yield and medium

Fig. 7 Production of H_2 and N_2 from hydrous hydrazine as a function of time in the presence of NaOH (0.5 M) at 25 ^{o}C using $Ni@SiO_2$ (black triangles), $Rh@SiO_2$ (blue circles), and $Rh/Ni@SiO_2$-3T (red squares) catalysts.

selectivity of 1.3 equiv and 42%, respectively, were observed. Moreover, the release of gases terminated after about 6.3 h. These results clearly demonstrate that the bimetallic alloy is crucial for high yield and selectivity. The RhNi bimetallic species anchored on the Ni surface appear to promote the adsorption of hydrous hydrazine so that complete decomposition of hydrous hydrazine into H_2 and N_2 predominantly occurs. Thus, the bimetallic hollow catalysts ($Rh/Ni@SiO_2$) clearly show a synergetic effect and superior catalytic activity compared to those of the monometallic congeners. Table S2 presents an overview of recently reported catalysts that efficiently produced hydrogen from hydrous hydrazine. Compared with other Rh alloy catalysts (entries 3 and 9), the $Rh/Ni@SiO_2$ catalyst shows excellent H_2 selectivity even at 25 ^{o}C despite of a low Rh content.

Because of the presence of magnetic Ni layers in the $Rh/Ni@SiO_2$ microsphere, the catalyst was separated simply by using a magnet after completion of the reaction (Fig. S5). A remarkable advantage of these catalysts is that they can be reused without loss of catalytic activity. The $Rh/Ni@SiO_2$-3T catalyst was recycled three times; the results are shown in Fig. 8. For the second cycle, the reaction provided a virtually identical yield of gases (2.99 equiv.). Even for the third cycle, the yield of gases released was 2.99 equiv although the reaction took slightly longer (2.0 h) than the first run. These results clearly demonstrate that the bimetallic NPs supported on hollow Ni-coated microspheres are highly resistant to deactivation in alkaline solution and retain excellent catalytic activity for the complete decomposition of hydrous hydrazine. Thus, hollow $Rh/Ni@SiO_2$-3T microspheres can be considered to be one of the most promising catalysts for hydrogen production from hydrous hydrazine in commercial applications.
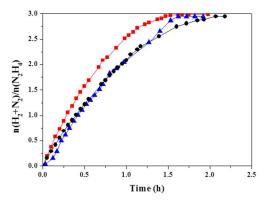

Fig. 8 Recycle test of the $Rh/Ni@SiO_2$-3T catalyst: Production of H_2 and N_2 from hydrous hydrazine as a function of time in the presence of NaOH (0.5 M) at 25 ^{o}C using a $Rh/Ni@SiO_2$-3T catalyst. The red squares, blue triangles, and black circles indicate the first, second, and third cycles, respectively. The used catalysts were separated by using a magnet after the reaction.

Conclusions

In conclusion, we developed a simple and efficient methodology for the synthesis of hollow Ni-coated microspheres ($Rh/Ni@SiO_2$) containing Rh NPs using core/shell silica microspheres as templates. The Ni-coated hollow microsphere with a low loading of Rh showed excellent catalytic performance for complete conversion of NH_2NH_2 into H_2 and N_2 at room temperature with over 99% H_2 selectivity. Our study highlights a method for the exclusive production of H_2 from NH_2NH_2 using a low-cost and recyclable catalyst under industrially realistic conditions, which opens up the possibility of accelerating the practical application of H_2NNH_2 as a hydrogen-storage material.

Acknowledgements

Notes and references

Department of Chemistry, Sogang University, Seoul 121-742 (Korea). E-mail: nhhur@sogang.ac.kr
† Electronic Supplementary Information (ESI) available: [details of any supplementary information available should be included here]. See DOI: 10.1039/b000000x/

1   Y. Xia, Z. Yang and Y. J. Zhu, *J. Mater. Chem. A*, 2013, **1**, 9365.
2   K. Shimura and H. Yoshida, *Energy Environ. Sci.*, 2011, **4**, 2467.

3   L. Schlapbach and A. Züttel, *Nature*, 2001, **414**, 353.

4   N. Armaroli and V. Balzani, *ChemSusChem*, 2011, **4**, 21.

5   J. B. O. Santos, G. P. Valenca and J. A. J. Rodrigues, *J. Catal.,* 2002, **210**, 1.

6   B. Sakintuna, F. Lamari-Darkrim and M. Hirscher, *Int. J. Hydrogen Energy*, 2007, **32**, 1121.

7   G. Moussa, R. Moury, U. Demirci, T. Sener and P. Miele, *Int. J. Energy Res.*, 2013, **37**, 825.

8   D. Teichmann, W. Arlt, P. Wasserscheid and R. Freymann, *Energy Environ. Sci.*, 2011, **4**, 2767.

9   L. Chong, J. Zou, X. Zeng and W. Ding, *J. Mater. Chem. A*, 2013, **1**, 3983.

10 S. S. Muir and X. Yao, *Int. J. Hydrogen Energy*, 2011, **36**, 5983.

11 J. Zhang, T. S. Fisher, J. P. Gore, D. Hazra and P. V. Ramachandran, *Int. J. Hydrogen Energy*, 2006, **31**, 2292.

12 H. Dai, Y. Liang, L. Ma and P. Wang, *J. Phys. Chem. C*, 2008, **112**, 15886.

13 H. I. Schlesinger, H. C. Brown, A. E. Finholt, J. R. Gilbreath, H. R. Hoekstra and E. K. Hyde, *J. Am. Chem. Soc.*, 1953, **75**, 215.

14 B. H. Liu and Z. P. Li, *J. Power. Sources*, 2009, **187**, 527.

15 M. J. F. Ferreira, L. Gales, V. R. Fernandes, C. M. Rangel and A. M. F. R. Pinto, *Int. J. Hydrogen. Energy*, 2010, **35**, 9869.

16 S. J. Cho, J. Lee, Y. S. Lee and D. P. Kim, *Catal. Lett.*, 2006, **109**, 181.

17 S. K. Singh and Q. Xu, *Catal. Sci. Technol.*, 2013, **3**, 1889.

18 H. Jiang, S. K. Singh, J. Yan, X. Zhang and Q. Xu, *ChemSusChem*, 2010, **3**, 541.

19 D. G. Tong, W. Chu, P. Wu, G. F. Gu and L. Zhang, *J. Mater. Chem. A*, 2013, **1**, 358.

20 E. W. Schmidt, *Hydrazine and Its Derivatives: Preparation, Properties, Applications.* Second Edition; John Wiley and Sons, Inc.: 2001; Vol. **1** and **2**.

21 L. He, Y. Huang, X. Y. Liu, L. Li, A. Wang, X. Wang, C. Mou and T. Zhang, *Appl. Catal. B: Environ.,* 2014, **147**, 779.

22 K. V. Manukyan, A. Cross, S. Rouvimov, J. Miller, A. S. Mukasyan and E. E. Wolf, *Appl. Catal. A: Gen.*, 2014, **476**, 47.

23 T. Umegaki, J. Yan, X. Zhang, H. Shioyama, N. Kuriyama and Q. Xu, *Int. J. Hydrogen Energy*, 2009, **34**, 2303.

24 A. K. Singh and Q. Xu, *Int. J. Hydrogen Energy,* 2014, **39**, 9128.

25 L. He, Y. Huang, A. Wang, X. Wang, X. Chen, J. J. Delgado and T. Zhang, *Angew. Chem. Int. Ed.*, 2012, **51**, 6191.

26 L. He, Y. Huang, A. Wang, X. Wang and T. Zhang, *AlChE. J.*, 2013, **59**, 4297.

27 L. He, Y. Huang, A. Wang, Y. Liu, X. Liu, X. Chen, J. J. Delgado, X. Wang and T. Zhang, *J. Catal.,* 2013, **298**, 1.

28 M. Yadav and Q. Xu, *Energy. Environ. Sci.*, 2012, **5**, 9698.

29 S. K. Singh, X. Zhang and Q. Xu, *J. Am. Chem. Soc.,* 2009, **131**, 9894.

30 S. K. Singh and Q. Xu, *Chem. Commun.*, 2010, **46**, 6545.

31 S. K. Singh, Z. Lu and Q. Xu, *Eur. J. Inorg. Chem.*, 2011, **2011**, 2232.

32 J. Zhang, Q. Kang, Z. Yang, H. Dai, D. Zhuang and P. Wang, *J. Mater. Chem. A*, 2013, **1**, 11623.

33 S. K. Singh, Y. Iizuka and Q. Xu, *Int. J. Hydrogen. Energy*, 2011, **36**, 11794.

34 S. K. Singh, A. K. Singh, K. Aranishi and Q. Xu, *J. Am. Chem. Soc.*, 2011, **133**, 19638.

35 D. G. Tong, D. M. Tang, W. Chu, G. F. Gu and P. Wu, *J. Mater. Chem. A*, 2013, **1**, 6425.

36 S. K. Singh and Q. Xu, *J. Am. Chem. Soc.*, 2009, **131**, 18032.

37 A. K. Singh, M. Yadav, K. Aranishi and Q. Xu, *Int. J. Hydrogen. Energy*, 2012, **37**, 18915.

38 J. Wang, X. Zhang, Z. Wang, L. Wang and Y. Zhang, *Energy. Environ. Sci.*, 2012, **5**, 6885.

39 C. Yan and D. Xue, *J. Phys. Chem. B.*, 2006, **110**, 7102.

40 X. W. Lou, L. A. Archer and Z. Yang, *Adv. Mater.*, 2008, **20**, 3987.

41 X. Gong, L. Wang and W. Wen, *Chem. Commun.*, 2009, **31**, 4690.

42 J. B. Yoo, H. J. Yoo, B. W. Lim, K. H. Lee, M. H. Kim, D. Kang and N. H. Hur, *ChemSusChem*, 2012, **5**, 2334.

43 E. Hemmer, N. Venkatachalam, H. Hyodo, A. Hattori, Y. Ebina, H. Kishimoto and K. Soga, *Nanoscale*, 2013, **5**, 11339.

44 C. Chen, L. K. Yee, H. Gong, Y. Zhang and R. Xu, *Nanoscale*, 2013, 5, 4314.

45 W. Di, S. K. P. Velu, A. Lascialfari, C. Liu, N. Pinna, P. Arosio, Y. Sakka and W. Qin, W. *J. Mater. Chem.*, 2012, 22, 20641.

46 Z. Xu, Y. Gao, T. Liu, L. Wang, S. Bian and J. Lin, *J. Mater. Chem.*, 2012, **22**, 21695.

47 Z. H. Zhang, L. Chen, Q. H. Gan, Q. Tian, C. L. Chen and Z. L. Huang, *Phys. Status. Solidi. A*, 2013, **210**, 378.

48 H. Qin, X. Zhang, H. Liu, Y. Sang and J. Wang, *CrystEngComm.*, 2013, **15**, 5076.

49 L. Su, C. Ma, T. Hou and W. Han, *RSC Adv.*, 2013, **3**, 19807.

50 P. Burattin, M. Che and C. Louis, *J. Phys. Chem. B*, 1997, **101**, 7060.

51 M. Khoudiakov, M. C. Gupta and S. Deevi, *Appl. Catal. A: Gen.*, 2005, **291**, 151.

52 J. A. Schwarz, *Chem. Rev.*, 1995, **95**, 477.

53 W. Stöber and A. Fink, *J. Colloid. Interface. Sci.*, 1968, **26**, 62.

54 T. T. Ngo, A. P. H. Phan, C. F. Yam and H. M. Lenhoff, *Anal. Chem.*, 1982, **54**, 46.

55 P. Moreno, E. Sánchez, A. Pons and A. Palou, *Anal. Chem.*, 1986, 58, 585.

56 E. Mavredaki, E. Neofotistou and K. D. Demadis, *Ind. Eng. Chem. Res.*, 2005, **44**, 7019.

57 S. Tomiyama, R. Takahashi, S. Sato, T. Sodesawa and S. Yoshida, *Appl. Catal. A: Gen.*, 2003, **241**, 349.

58 R. Nakamura and H. Nakajima, *J. Phys.: Conf. Ser.* 2009, **165**, 012072.

59 R. Nakamura, D. Tokozakura, J. Lee, H. Mori and H. Nakajima, *Acta. Mater.*, 2008, **56**, 5276.

60 J. Gao, C. Jia, M. Zhang, F. Gu, G. Xu and F. Su, *Catal. Sci. Technol.*, 2013, **3**, 2009.

61 A. Jangam and S. Kawi, *ACS. Catal.*, 2014, **4**, 289.

62 S. Wang, X. Guo, H. Yang, J. Dai, R. Zhu, J. Gong, L. Peng, W. Ding, *Appl. Surface. Sci.*, 2014, **288**, 530.

63 Y. Luo, J. Zhang, Y. Shen, S. Jiang and G. Liu, *J. Mater. Sci. Technol.*, 2007, **5**, 587.

64 H. Jiang, T. Umegaki, T. Akita, X. Zhang, M. Haruta and Q. Xu, *Chem. Eur. J.*, 2010, **16**, 3132.

65 K. S. Han and O. H. Han, *Bull. Korean Chem. Soc.*, 2006, **26**, 1121.

66 Y. Hou and S. Gao, *J. Alloys. Compd.*, 2004, **365**, 112.

67 F. Liu, J. Y. Lee and W. Zhou, *J. Phys. Chem. B*, 2004, **108**, 17959.

68   A. P. Grosvenor, M. C. Biesinger, R. St. C. Smart and N. S. McIntyre, *Surf. Sci.*, 2006, **600**, 1771.

69   L. Xia, X. Hu, X. Kang, H. Zhao, M. Sun and X. Cihen, *Coll. Surf. A: Physicochem. Eng. Aspects*, 2010, **367**, 96.

70   H. B. Li, M. H. Yu, F. X. Wang, P. Liu, Y. Liang, J. Xiao, C. X. Wang, Y. X. Tong and G. W. Yang, *Nat. Commun.*, 2013, **4**, 1894.

71   L. Mi, Q. Ding, W. Chen, L. Zhao, H. Hou, C. Liu, C. Shen and Z. Zheng, *Dalton Trans.*, 2013, **42**, 5724.

72   Z. Xu, J. Yu, G. Liu, B. Cheng, P. Zhou and X. Li, *Dalton Trans.*, 2013, **42**, 10190.

73   J. Yang, X. Duan, Q. Qin and W. Zheng, *J. Mater. Chem. A*, 2013, 1, 7880.

74   G. He, G. W. Meng, L. D. Zhang and M. Liu, *Appl. Phys. Lett.*, 2007, **91**, 232910.

75   S. N. Arafat, S. Dutta, M. Perring, M. Mitchell, P. J. A. Kenis and N. B. Bowden, *Chem. Commun.*, 2005, 3198.

76   T. D. Shen, I. Shmagin, C. C. Koch, R. M. Kolbas, Y. Fahmy, L. Bergman, R. J. Nemanich, M. T. McClure, Z. Sitar and M. X. Quan, *Phys. Rev. B*, 1997, **55**, 7615.

77   H. Lin, S. Wong, C. Mou and C. Tang, *J. Phys. Chem. B*, 2000, **104**, 8967.

78   J. Li, J. Lin, X. Xu, X. Zhang, Y. Xue, J. Mi, Z. Mo, Y. Fan, L. Hu, X. Yang, J. Zhang, F. Meng, S. Yuan and C. Tang, *Nanotechnology*, 2013, **24**, 155603.

79   R. Jia, J. Chen, J. Zhao, J. Zheng, C. Song, L. Li and Z. Zhu, *J. Mater. Chem.*, 2010, **20**, 10829.

80   Y. Liang, D. Wu and R. Fu, *Sci. Rep.*, 2013, **3**, 1119.

81   S. Feng, W. Li, Q. Shi, Y. Li, J. Chen, Y. Ling, A. M. Asiri and D. Zhao, *Chem. Commun.*, 2014, DOI: 10.1039/C3CC46492J.

Journal of Materials Chemistry A Accepted Manuscript

Table of Contents (TOC) Graphic

Hollow nickel-coated microspheres containing Rh nanoparticles (Rh/Ni@SiO$_2$) generates hydrogen (H$_2$) from hydrazine (H$_2$NNH$_2$) with over 99% selectivity within 1.5 h at 25 ^{o}C